ACCSCIENCE PUBLISHING

Materials Science in Additive Manufacturing

ORIGINAL RESEARCH ARTICLE

A hybrid 3D-printed/electrospun biodegradable drug-eluting scaffold for heterotopic ossification-related local drug delivery

Chih-Yang Lai[1,2], Po-Ju Lai[1,2], Szu-Yao Wang[1,2], Zi-He Kuo[1], Ulfia Nur Amallia[1], I-Lan Fan[1], and Shih-Jung Liu[1,2]*

[1]Department of Mechanical Engineering, Chang Gung University, Taoyuan, Taiwan

[2]Bone and Joint Research Center, Department of Orthopedics, Chang Gung Memorial Hospital at Linkou, Taoyuan, Taiwan

Abstract

Heterotopic ossification (HO) is a clinically challenging complication after trauma or orthopedic surgery. This study evaluated a hybrid biodegradable scaffold for localized peri-osseous delivery of agents relevant to HO-risk and bone-healing environments. Polycaprolactone (PCL) mesh scaffolds were fabricated using solvent-cast additive manufacturing as flexible macro-scale barriers, while poly(lactic-co-glycolic acid) (PLGA) nanofibers incorporating indomethacin, teicoplanin, and bone morphogenetic protein-2 (BMP-2) were prepared using electrospinning and coaxial electrospinning. Scaffold morphology, wettability, mechanical behavior, Fourier-transform infrared spectroscopy and differential scanning calorimetry profiles, *in vitro* release, rabbit local/systemic release, and peri-implant histology were evaluated. The PCL mesh showed an ultimate tensile strength of 26.2 ± 2.6 MPa and a maximum strain of 337%. After 3 days in phosphate-buffered saline, the assembled PCL mesh/PLGA nanofiber scaffold retained comparable tensile properties, with an ultimate tensile strength of 24.8 ± 2.0 MPa and maximum strain of 334 ± 6%, indicating preserved flexibility under hydrated conditions. Drug-loaded PLGA nanofibers showed reduced tensile strength compared with pristine PLGA fibers, indicating that drug incorporation affected nanofiber handling and durability. *In vitro* testing demonstrated initial burst release of indomethacin and teicoplanin followed by sustained release, whereas BMP-2 release persisted for more than 30 days. In healthy rabbits, local teicoplanin and indomethacin levels were sustained for 28 days with substantially lower systemic levels. Histology demonstrated an early peri-implant inflammatory response that decreased over time. As no validated HO model or ectopic bone quantification was used, the findings support scaffold feasibility and localized delivery, not proven HO prevention. Further disease-model efficacy, biological activity, dose optimization, degradation, and safety studies are required before clinical translation.

Keywords: Heterotopic ossification; Drug-eluting scaffold; 3D printing; Electrospinning; Localized drug delivery; Release characterization

***Corresponding author:**
Shih-Jung Liu
(shihjung@mail.cgu.edu.tw)

Citation: Lai CY, Lai PJ, Wang SY, *et al*. A hybrid 3D-printed/electrospun biodegradable drug-eluting scaffold for heterotopic ossification-related local drug delivery. *Mater Sci Add Manuf.* 2026;5(3):026220049. doi: 10.36922/MSAM026220049

Received: May 25, 2026

Revised: June 10, 2026

Accepted: June 16, 2026

Published online: July 10, 2026

1. Introduction

Heterotopic ossification (HO) is a pathological condition in which bone abnormally forms within soft tissues where bone normally should not develop.[1,2] It often occurs in response to trauma, surgery, or as a complication of certain medical conditions such as burns, spinal cord injury, or orthopedic surgeries. Previous studies have reported that HO is particularly common in patients with specific risk factors.[1,2] HO frequently develops after orthopedic procedures—especially hip arthroplasty, where rates can approach ~40%. It is also seen following fractures or dislocations (up to ~30%), with elbow injuries being a frequent site. The risk increases further after high-energy limb trauma and in neurologic conditions such as traumatic brain injury or spinal cord injury, with HO reported in as many as ~50% of spinal cord injury cases. Severe burns are another trigger, with rates up to ~20% in third-degree burns. In the setting of severe traumatic amputations, the incidence can exceed 90%. These abnormal bone formations can lead to pain, restricted joint movement, and impaired function, significantly impacting a patient's quality of life. While the exact mechanisms underlying HO are not fully understood, inflammation, tissue injury, and dysregulated bone morphogenetic protein signaling are believed to play key roles.[3-5]

Heterotopic ossification can lead to pain, stiffness, and functional impairment. The treatment approach depends on the severity of symptoms and the impact on the patient's mobility and quality of life. Non-surgical management is often the first line of treatment, particularly in early or mild cases.[6,7] Medications such as nonsteroidal anti-inflammatory drugs (NSAIDs), including indomethacin, are widely employed to inhibit abnormal bone formation. In cases where non-surgical approaches are insufficient, surgical intervention may be necessary. Ectopic bone excision is the primary surgical option for patients experiencing significant pain or functional limitations. Radiation therapy is another option, particularly for preventing HO in high-risk patients. Low-dose radiation, administered pre- or postoperatively, is effective in reducing the likelihood of HO formation following surgeries like hip arthroplasty. Despite these treatment methods, HO remains a challenge for the patients.[8-10]

Tissue engineering and local drug-delivery strategies may provide an adjunctive approach for high-risk peri-osseous environments where inflammation, infection risk, mechanical irritation, and bone repair coexist.[11-13] For the specific context of HO prophylaxis, an ideal implantable platform would have several features: (i) sufficient flexibility and mechanical integrity to conform to complex bone surfaces and soft-tissue planes; (ii) a macro-scale barrier component to separate periosteal and soft-tissue compartments; (iii) localized delivery of pharmacologic agents that may reduce inflammation or infection risk while limiting systemic exposure; and (iv) biodegradability to avoid a second removal procedure. However, demonstrating true HO prevention requires disease-relevant animal models and direct quantification of ectopic bone; material fabrication and release studies alone cannot establish anti-HO efficacy.

In this work, we developed a hybrid biodegradable scaffold consisting of a three-dimensionally (3D) printed polycaprolactone (PCL) mesh and multilayer poly(lactic-co-glycolic acid) (PLGA) nanofibrous membranes. The intended technical contribution is the integration of a flexible printed barrier with electrospun drug-loaded nanofibers and coaxially electrospun bone morphogenetic protein 2 (BMP-2)-containing fibers in a single peri-osseous platform. The study objective was to characterize fabrication feasibility, physicochemical properties, mechanical behavior, and local release profiles, rather than to directly prove suppression of HO formation.

Indomethacin was selected because NSAIDs are commonly used for HO prophylaxis and can reduce prostaglandin-mediated inflammatory signaling. Teicoplanin was incorporated as a locally delivered glycopeptide antibiotic to address infection risk in trauma or implant-related settings. BMP-2 was included to explore whether a spatially compartmentalized scaffold could also provide a bone-healing signal; however, BMP-2 is osteoinductive and may theoretically promote ectopic ossification if released into surrounding soft tissues. Therefore, the BMP-2 component should be regarded as an exploratory design feature that requires careful spatial/temporal control and further biological validation before any anti-HO claim can be made.

After fabrication, the mechanical properties of the printed PCL mesh, spun PLGA nanofibrous mats, and assembled PCL mesh/PLGA nanofiber hybrid scaffold were measured, including wet-state tensile testing of the assembled hybrid construct after phosphate-buffered saline (PBS) immersion. Morphology, wettability, Fourier transform infrared spectroscopy (FTIR), and differential scanning calorimetry (DSC) were used to characterize scaffold structure and drug incorporation. *In vitro* release characteristics of indomethacin, teicoplanin, and BMP-2 were evaluated using elution assays, high-performance liquid chromatography (HPLC), and enzyme-linked immunosorbent assay (ELISA), while *in vivo* release of indomethacin and teicoplanin from the hybrid scaffold was assessed in a healthy rabbit implantation model.

The novelty of the present study does not lie in the individual use of PCL, PLGA electrospinning, coaxial electrospinning, or local drug delivery, all of which have been previously reported. Rather, the main contribution is the integrated scaffold architecture that combines a conformable macro-scale 3D-printed PCL barrier with multilayer electrospun PLGA drug-delivery compartments for localized peri-osseous application in HO-related settings.

2. Materials and methods

2.1. Materials

The polymers used were PCL (molecular weight: 80,000 Da) and PLGA with a lactic acid-to-glycolic acid ratio of 50:50 (molecular weight: 33,000 Da). Dichloromethane and hexafluoro-2-propanol (HFIP) were utilized as solvents, while the drugs and the biomolecule employed were commercially available indomethacin, teicoplanin, and BMP-2. All materials were sourced from Sigma-Aldrich (United States of America [USA]).

2.2. Manufacture of biodegradable polycaprolactone mesh scaffold

To prepare biodegradable PCL meshes, a solvent-cast additive manufacturing device was employed. The device consisted of a solution-extrusion feeder, stepper motors and associated parts, a power supply, a syringe, a dispensing tip with an inner diameter of 0.18 mm at the outlet, a collection platform, and a user interface (Figure 1A).[14] The entire fabrication process was controlled using Ultimaker Cura software (version 4.13.1, Ultimaker B.V., The Netherlands).

Before printing, 1,680 mg of PCL was mixed with 2.36 mL of dichloromethane and blended by stirring for 2 h. The prepared solution was then loaded into the manufacturing system for processing. A microprocessor-controlled servo motor regulated the feeder, which dispensed the PCL mixture layer by layer onto the collection plate. Following solvent evaporation, bioresorbable mesh scaffolds with a pore size of 3 mm (Figure 1B) were successfully deposited on the collection platform.

2.3. Electrospinning of nanofibrous membranes

A tri-layer nanofiber membrane comprising two drug-loaded electrospun layers and one BMP-2-loaded coaxial layer was prepared. To fabricate the first layer, PLGA (1,840 mg) and teicoplanin (280 mg) were dissolved in 4 mL of HFIP and electrospun into nanofibers using a laboratory-fabricated electrospinning device. The solution was delivered at 0.4 mL/h. The applied voltage was set to 18 kV, and the needle-to-collector distance was 15 cm. The electrospinning of the second layer followed the same procedure, except that the teicoplanin was replaced by indomethacin.

To prepare the third layer, PLGA (1,120 mg) was dissolved in 4 mL of HFIP to form the sheath solution. The core solution consisted of BMP-2 (20 mg) blended with 1 mL of PBS and 1 µL of bovine serum albumin solution (0.1% [w/v]; Sigma-Aldrich, USA). The mixtures were then loaded into two separate syringe–needle assemblies for coaxial electrospinning. The inner diameters of the needles for the sheath and core layers were 1.20 mm and 0.43 mm, respectively. The sheath-solution flow rate was 0.9 mL/h, and the core-solution flow rate was 0.3 mL/h. The voltage was maintained at 18 kV, and the needle-to-collector distance was 15 cm.

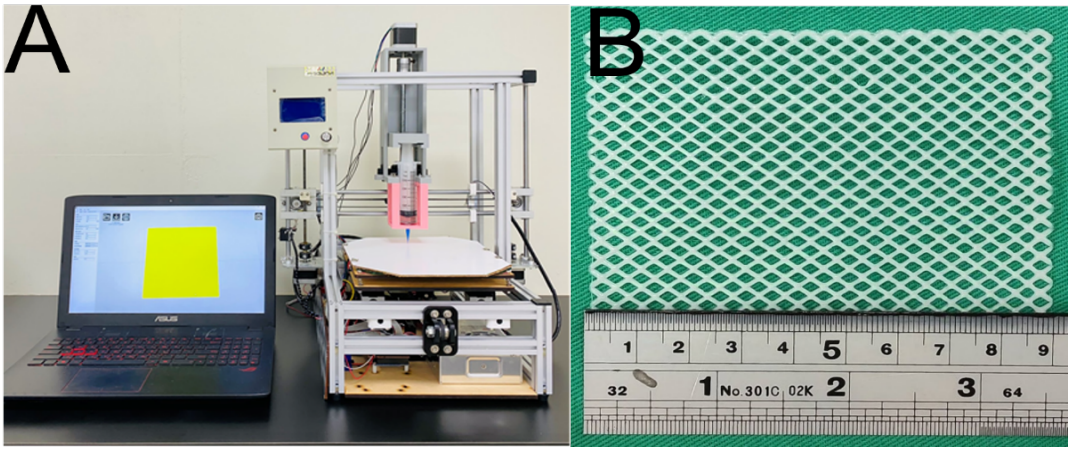

Figure 1. The solvent-cast additive manufacturing device (A) and additively manufactured polycaprolactone mesh (B)

All electrospinning was carried out at room temperature. The resulting tri-layer nanofibrous mats had a thickness of approximately 200 μm. After fabrication, the mats were vacuum-dried at 40 °C for 72 h to remove residual solvent.

2.4. Morphological characterization

The morphology of the fabricated nanofibers was examined by scanning electron microscopy (Jeol 7500F, Tokyo, Japan) after gold sputter coating.

2.5. Mechanical properties

The mechanical strengths of the PCL mesh, PLGA nanofibers, and assembled hybrid scaffolds were measured using a tensiometer (LR5KPlus, Lloyd, USA). Specimens were pulled at a rate of 60 mm/min. The maximum load, tensile strength, stress-strain behavior, and elongation at break were recorded, and measurements were performed in triplicate (n = 3) for each tested material. To address the mechanical behavior of the final assembled construct, additional tensile testing was performed on hybrid scaffold specimens consisting of the 3D-printed PCL mesh combined with PLGA nanofibrous membranes. The hybrid specimens were submerged in PBS at 37 °C for 3 days before testing to simulate a hydrated implantation environment. For benchmark comparison, PCL mesh-only specimens were evaluated using the same tensile protocol. Ultimate tensile stress, stress-strain behavior, and maximum strain were recorded for comparison between the PCL mesh and the assembled hybrid scaffold.

2.6. Water contact angle

The water contact angles of electrospun nanofibers were determined through a water contact angle analyzer (FTA125, First Ten Angstroms, USA). Samples (1 cm × 1 cm) were cut from the nanofibrous mats and placed on the testing stage. A droplet of distilled water was carefully deposited onto each sample surface. The contact angles were assessed using a video monitor. The contact angles of pristine PLGA and drug- and BMP-2-loaded PLGA nanofibers were assessed.

2.7. Fourier transform infrared assay

An FTIR spectrometer (Nicolet-iS5, Thermo-Fisher, USA) was employed to characterize the spectra of both pristine and drug-loaded nanofibers, with a resolution of 4 cm^{-1} and 32 scans. PLGA nanofibrous samples were pressed into KBr discs, and spectra were monitored over the 400–4,000 cm^{-1} range.

2.8. Differential scanning calorimetry

Differential scanning calorimetry measurements were performed to assess the thermal behavior of pristine PLGA and the drug-loaded PLGA nanofibers. The specimens were heated from 30–300 °C at a rate of 10 °C/min using a DSC instrument (DSC Q20, TA Instruments, DE, USA).

2.9. *In vitro* release profiles of drugs and biomolecules

An elution procedure was used to assess the *in vitro* release profiles of indomethacin, teicoplanin, and BMP-2 from the loaded nanofibrous mats. Individual nanofibrous samples (n = 3) were placed into separate test tubes containing 1 mL of PBS (0.15 mol/L, pH 7.4). The tubes were incubated at 37 °C for 24 h, and the resulting eluates were then collected for analysis. This procedure was repeated daily for 30 days, with each sample replenished with 1 mL of fresh PBS.

Drug levels in the eluates were determined by HPLC using a Mightysil RP-18 GP column (150 mm × 4.6 mm, 5 μm; Kanto Chemical Co., Inc., Japan) and a Hitachi L-2200R multi-solvent delivery system (Hitachi High-Technologies Corporation, Japan). For teicoplanin, the mobile phase consisted of acetonitrile and sodium acetate buffer (70:30, v/v), with detection at 260 nm and a flow rate of 1.3 mL/min. For indomethacin, an Inertsil C8 column (250 mm × 4.6 mm, 5 μm; GL Sciences Inc., Japan) was used, with distilled water and acetonitrile (70:30, v/v) as the mobile phase, detection at 254 nm, and a flow rate of 0.8 mL/min. BMP-2 concentrations were measured daily using an ELISA kit (DBP200, R&D Systems, Inc., USA).

2.10. *In vivo* release

Six adult New Zealand white rabbits (3.0 ± 0.5 kg) were used in this study (Livestock Research Institute, Ministry of Agriculture, Tainan, Taiwan). All animal procedures were approved by the Institutional Animal Care and Use Committee of Chang Gung University (IACUC No.: CGU113-178), in compliance with the regulations set by the National Institutes of Health of Taiwan. The rabbits were housed under veterinarian supervision in accordance with institutional regulations and the relevant regulations of the Taiwan Ministry of Health and Welfare. Animals were acclimatized before surgery, monitored daily for general appearance, wound condition, food intake, behavior, and signs of pain or distress, and received perioperative care according to institutional animal-care protocols. Humane endpoints included severe wound complications, persistent infection, marked weight loss, inability to ambulate or feed, or distress not relieved by veterinary intervention. No human subjects were involved in this study.

Anesthesia was induced in all rabbits by isoflurane inhalation in an anesthesia chamber and maintained with a mask for the duration of the operation. Under aseptic conditions, a longitudinal incision was made over the left lateral thigh, followed by extensive periosteal dissection

to expose the left femoral shaft. The 3D-printed mesh and electrospun nanofibers loaded with indomethacin, teicoplanin, and BMP-2 were first overlapped and then wrapped around the femoral shaft. The wound was then closed (Figure 2).

At days 1, 3, 7, 14, 21, and 28 post-implantation, tissues surrounding the implanted mesh/nanofibers and blood samples from the marginal ear veins were collected. Drug concentrations were measured using an HPLC assay.

2.11. Histological examination

At selected post-implantation time points, peri-implant soft tissue samples were collected from around the implanted hybrid scaffold for histological examination. No bone tissue was harvested for histological analysis. The collected soft tissue specimens were fixed in 10% neutral buffered formalin, dehydrated through a graded ethanol series, embedded in paraffin, and sectioned at a thickness of 5 μm. The sections were then stained with hematoxylin and eosin (H&E) according to standard histological protocols. A descriptive histological evaluation was performed to assess the local tissue response, including inflammatory cell infiltration and peri-implant tissue morphology. No quantitative histological scoring, immunohistochemical staining, mineralization-specific staining, or decalcification was performed. The reagents used for fixation and H&E staining were obtained from Sigma-Aldrich (USA).

2.12. Statistics and data analysis

Data are presented as mean ± standard deviation where applicable. This was an exploratory fabrication and release-characterization study with small sample sizes. Given the exploratory design and small sample sizes, release profiles and histological findings were analyzed descriptively. No formal statistical comparisons were performed. For time-dependent release data, results are primarily presented descriptively as daily concentration and cumulative release profiles because repeated-measure modeling was not prespecified. The limited sample size and exploratory statistical approach are acknowledged as limitations.

3. Results

3.1. 3D-printed polycaprolactone meshes

A biodegradable PCL mesh scaffold was successfully manufactured using the lab-developed solvent-cast 3D printing device, as shown in Figure 1B. The mechanical behavior of both the PCL mesh alone and the assembled hybrid scaffold was evaluated by tensile testing. As shown in Figure 3, the PCL mesh exhibited an ultimate tensile strength of 26.2 ± 2.6 MPa and a maximum strain of approximately 337% before failure, indicating high flexibility and extensibility. To better characterize the final construct intended for peri-osseous implantation, additional wet-state tensile testing was performed on the assembled PCL mesh/PLGA nanofiber hybrid scaffold after immersion in PBS for 3 days (Figure 4). The hybrid scaffold showed a stress-strain profile broadly comparable to that of the PCL mesh alone, with a slightly lower plateau stress but preserved elongation capacity. The hybrid scaffold exhibited an ultimate tensile strength of 24.8 ± 2.0 MPa and a maximum strain of 334 ± 6%. Compared with the PCL mesh alone, the assembled hybrid scaffold retained approximately 95% of ultimate tensile strength and nearly equivalent elongation capacity. These findings suggest that incorporation of the PLGA nanofibrous membrane did not substantially compromise the flexibility or tensile integrity of the PCL mesh backbone under hydrated conditions.

3.2. Drug-/biomolecule-loaded nanofibers

Drug- and BMP-2-loaded nanofibers were effectively fabricated using electrospinning and coaxial electrospinning techniques. Figure 5A–D shows the scanning electron microscopy images and fiber size distributions of pristine PLGA nanofibers, teicoplanin-loaded, indomethacin-loaded, and BMP-2-loaded nanofibers, respectively. The drug-loaded PLGA nanofibers exhibited smaller fiber

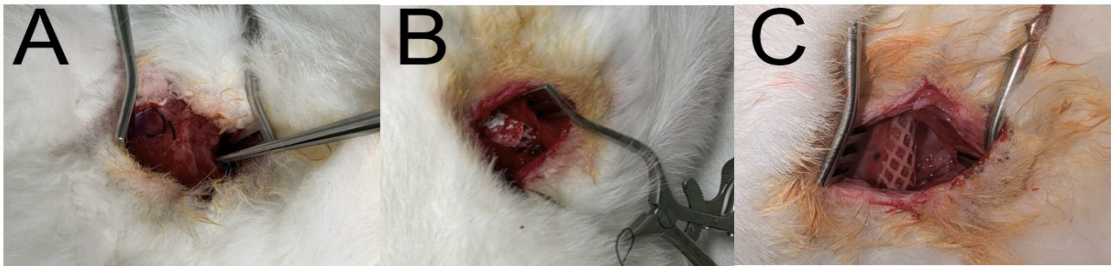

Figure 2. Photographs of the surgical procedure: (A) Exposure of the bone shaft; (B) implantation of the polycaprolactone mesh and drug-loaded nanofibers on day 0; (C) on day 28 post-implantation, the polycaprolactone mesh was visible, while the nanofibers had largely degraded

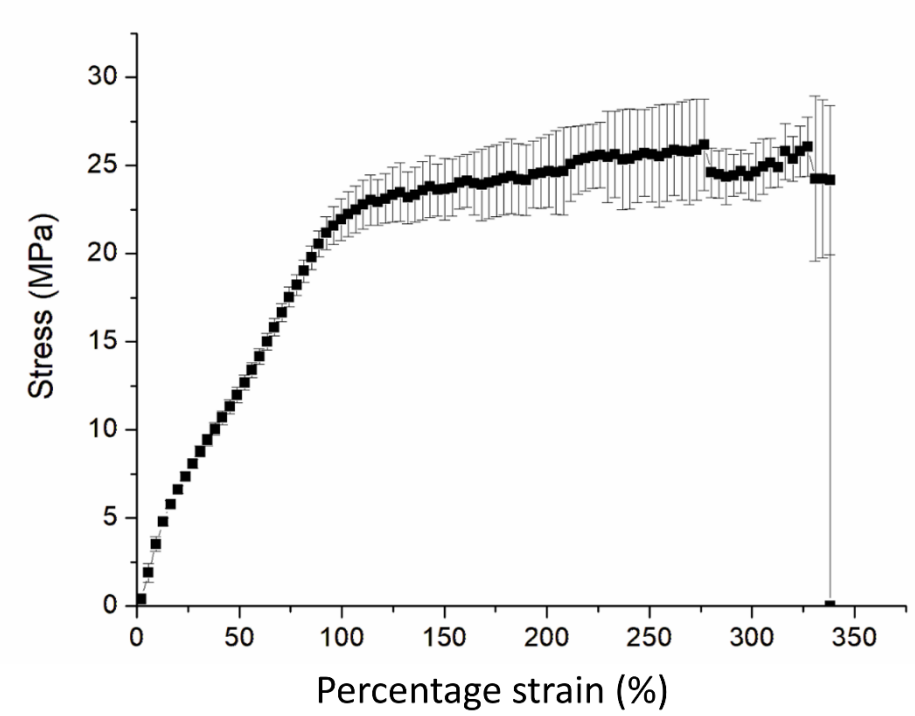

Figure 3. Stress–strain curves of 3D-printed polycaprolactone mesh specimens. Data are presented as mean ± standard deviation (n = 3).

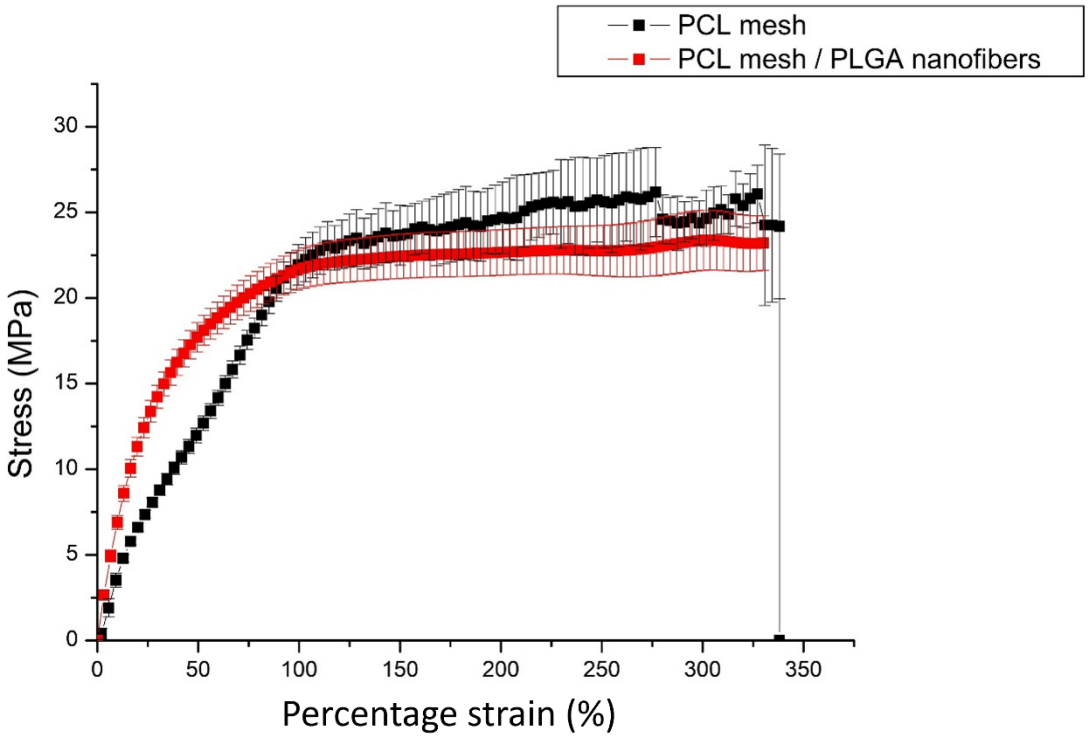

Figure 4. Stress–strain curves of the 3D-printed polycaprolactone (PCL) mesh and assembled PCL mesh/poly(lactic-co-glycolic acid) (PLGA) nanofiber hybrid scaffold. The hybrid scaffold specimens were submerged in phosphate-buffered saline at 37 °C for 3 days before tensile testing to simulate a hydrated environment. The hybrid scaffold exhibited an ultimate tensile strength of 24.8 ± 2.0 MPa and a maximum strain of 334 ± 6%, indicating preserved flexibility and tensile integrity compared with the PCL mesh alone. Data are presented as mean ± standard deviation (n = 3).

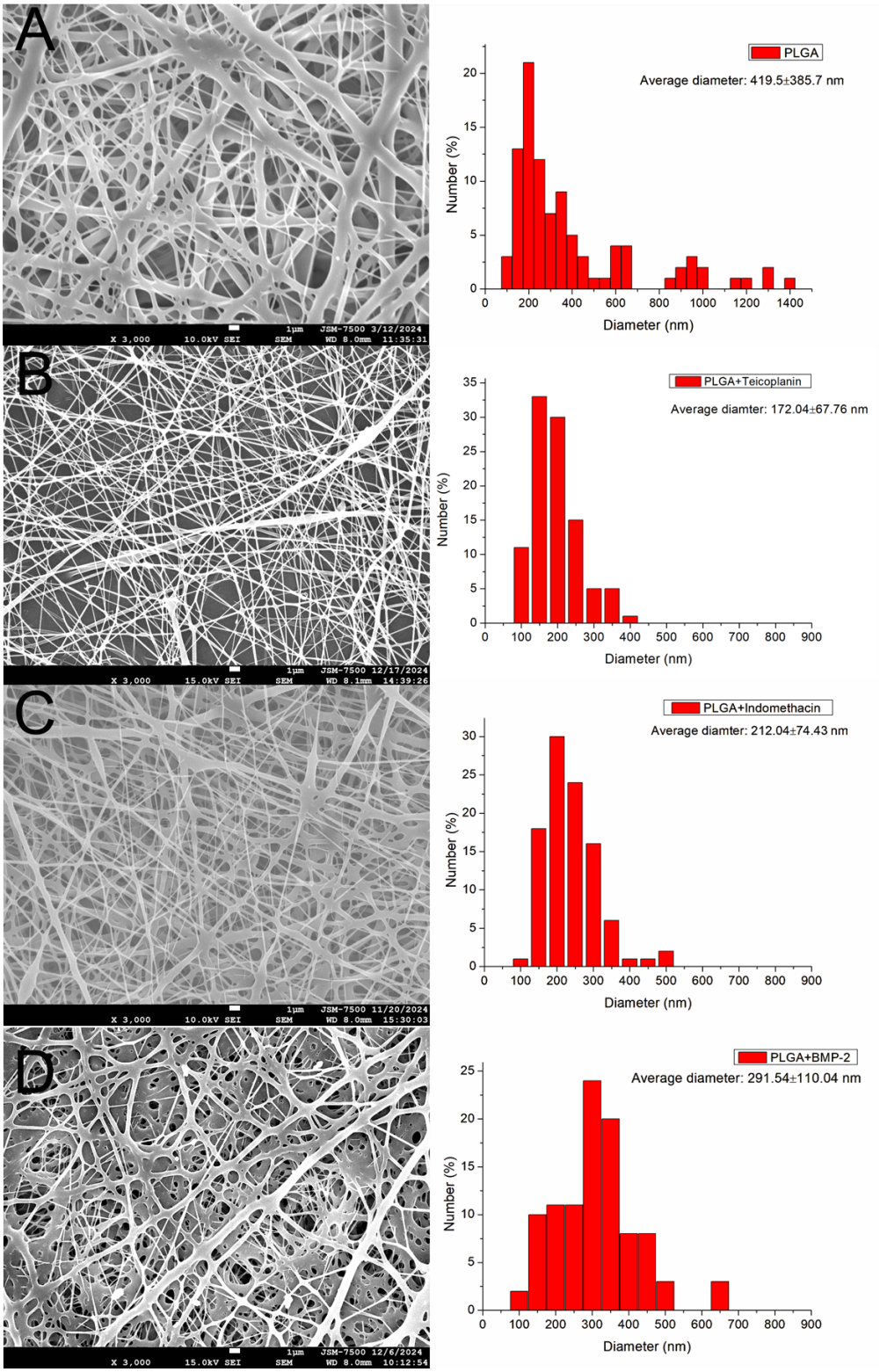

Figure 5. Scanning electron microscopy images and fiber size distributions of (A) pristine poly(lactic-co-glycolic acid) (PLGA), (B) PLGA/teicoplanin, (C) PLGA/indomethacin, and (D) PLGA/bone morphogenetic protein 2 (BMP-2) nanofibers. Scale bars: 1 μm; magnification: 3,000×.

diameters compared to the pristine PLGA nanofibers. During the electrospinning process, the polymeric material acts as a resistive force against external stretching caused by the electric field. The incorporation of pharmaceuticals in the fibers decreased the polymer content in the matrix, thereby decreasing the fibers' resistance to stretching. As a result, the fibers were more easily stretched, leading to a reduction in diameter. Meanwhile, due to the sheath-core structure, the BMP-2-loaded nanofibers displayed slightly larger diameters than the other drug-loaded nanofibers.

The wetting angles of pristine PLGA nanofibers, teicoplanin-loaded, indomethacin-loaded, and BMP-2-loaded nanofibers are shown in Figure 6, corresponding to 127.92°, 88.56°, 111.05°, and 100.50°, respectively. The addition of highly water-soluble teicoplanin markedly enhanced the hydrophilic properties of the fabricated nanofibrous mats. However, the low water solubility of indomethacin did not substantially affect the hydrophilicity of the PLGA nanofibers. Additionally, the BMP-2-loaded nanofibers, due to their sheath layer being composed of pristine PLGA, exhibited lower hydrophilicity.

The mechanical strengths of drug-eluting nanofibers were investigated. The tensile strengths shown in Figure 7 indicate that the drug-loaded nanofibers exhibited lower strengths compared to the pristine nanofibers. In a polymer–drug mixture, the polymer serves to resist external forces. Increasing the drug content decreased the relative proportion of polymer in the composite fibers, leading to a corresponding decrease in mechanical strength. Nevertheless, the indomethacin-loaded nanofibers displayed greater strain to failure relative to the pristine nanofibers and the teicoplanin-loaded nanofibers.

Figure 8A compares the FTIR spectra of pristine PLGA and PLGA loaded with teicoplanin. The spectrum of pristine PLGA shows the characteristic absorption peaks associated with the polymer backbone, while the teicoplanin-loaded sample exhibits additional or enhanced peaks. In particular, the spectrum displays distinct absorptions in the region associated with C=C stretching vibrations, at ~1,600 cm^{-1}, as indicated by the blue dashed lines. Additional peaks appear between ~1,100 and 900 cm^{-1}, corresponding to functional groups present in teicoplanin.[15,16] Figure 8B presents the spectra of pristine PLGA and PLGA incorporated with indomethacin.

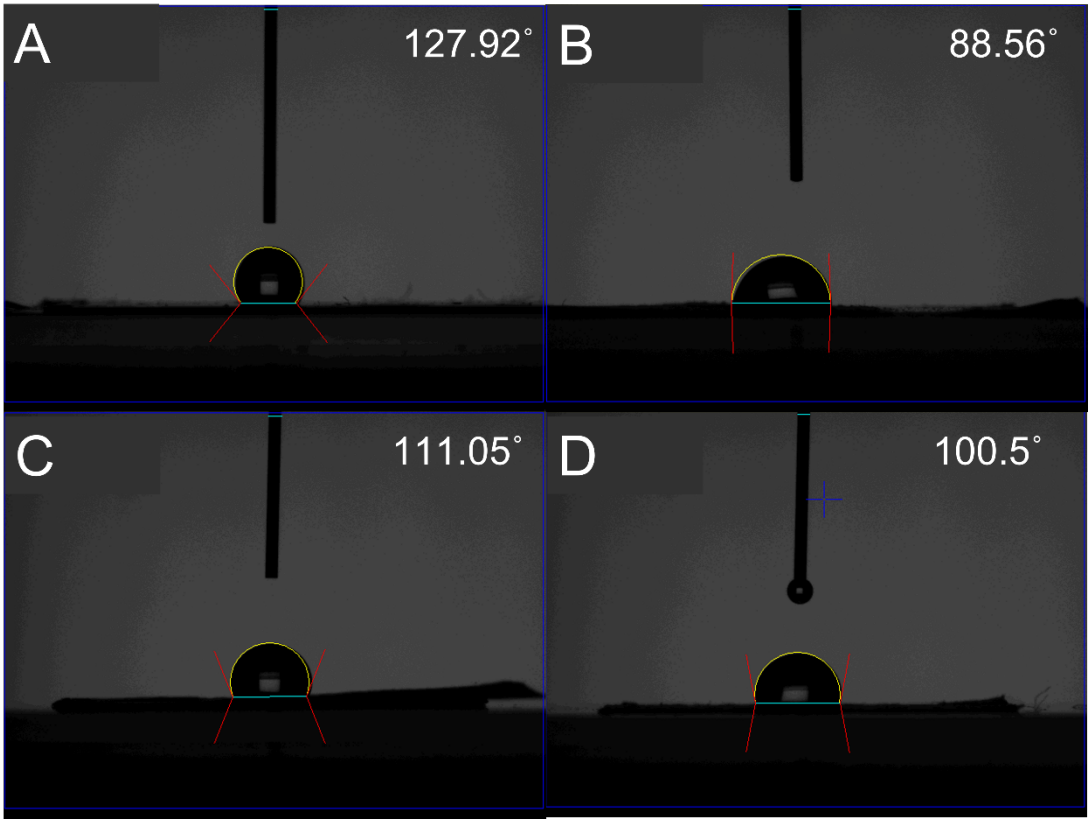

Figure 6. Hydrophilicity of (A) pristine poly(lactic-co-glycolic acid) (PLGA), (B) PLGA/teicoplanin, (C) PLGA/indomethacin, and (D) PLGA/bone morphogenetic protein 2 nanofibers

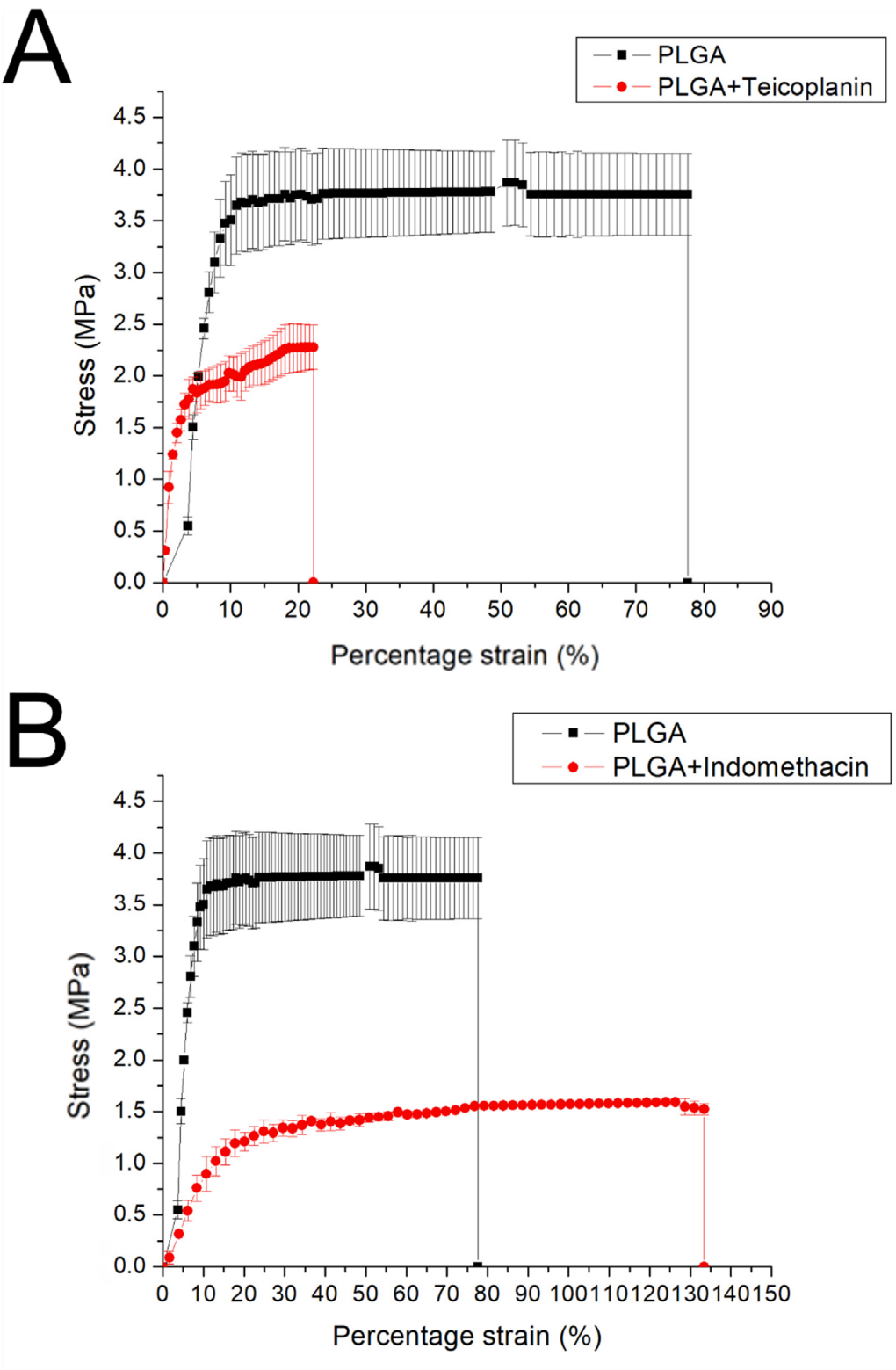

Figure 7. Stress–strain curves of (A) poly(lactic-co-glycolic acid) (PLGA)/teicoplanin and (B) PLGA/indomethacin nanofibers

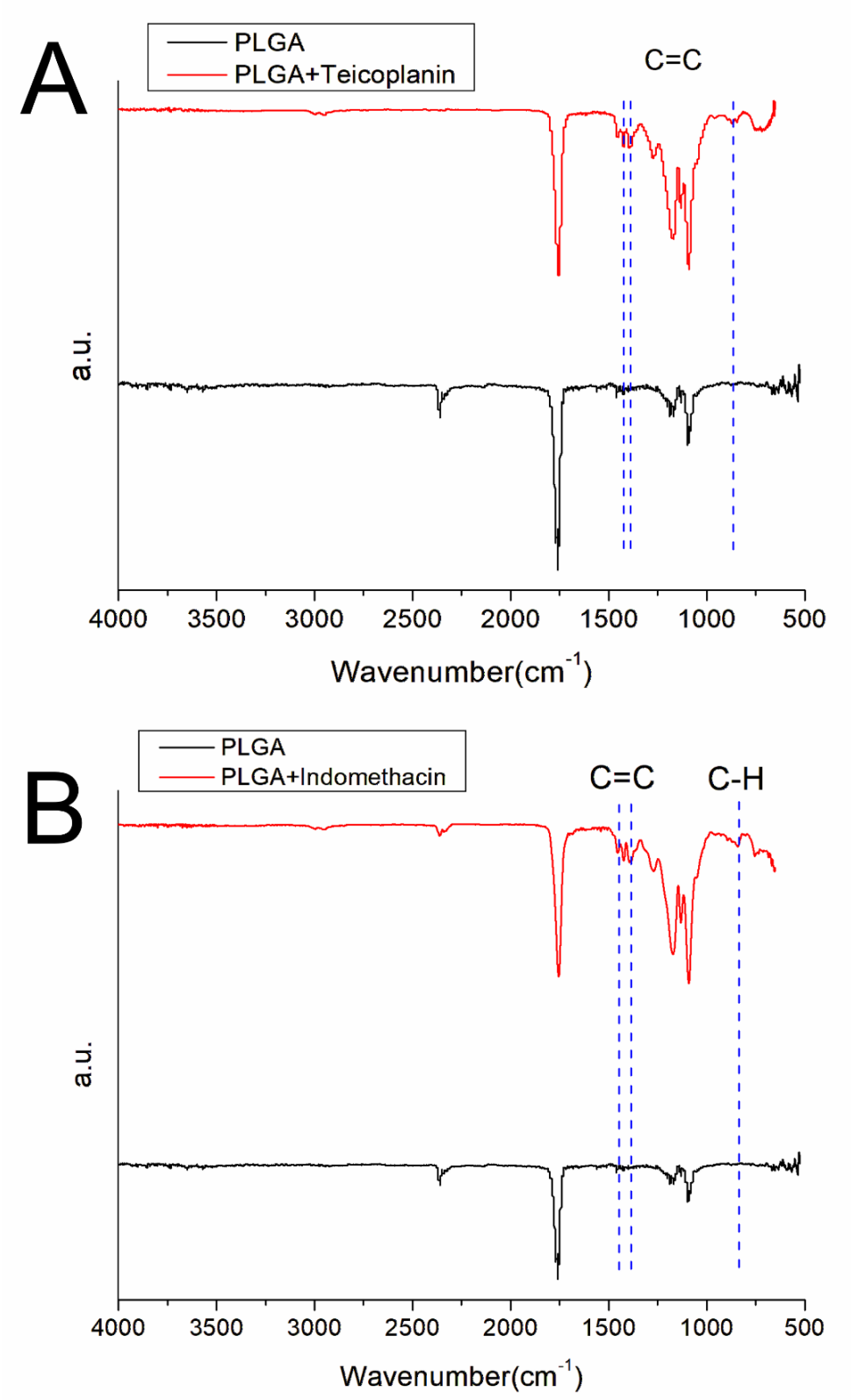

Figure 8. Fourier transform infrared spectra of (A) poly(lactic-co-glycolic acid) (PLGA)/teicoplanin and (B) PLGA/indomethacin nanofibers

The indomethacin-loaded spectrum exhibits noticeable additional bands. Distinct C=C stretching signals are again highlighted at ~1,600 cm^{-1}, while a second group of peaks around ~900 to 700 cm^{-1} corresponds to C–H bending modes.[17,18]

Figure 9A shows the DSC thermograms of pristine PLGA (black), teicoplanin (green), and PLGA loaded with teicoplanin (red). Pristine PLGA displays a smooth thermogram without a distinct melting peak, consistent with its amorphous nature. In contrast, teicoplanin alone exhibits a strong endothermic peak centered at approximately 150 °C, corresponding to its crystalline melting transition.[19] When teicoplanin is incorporated into PLGA, the thermogram of the composite shows no sharp melting peak. The disappearance of teicoplanin's crystalline endotherm suggests that the drug is molecularly dispersed or amorphously distributed within the PLGA matrix rather than present as crystalline domains. Figure 9B presents DSC curves for pristine PLGA, pristine indomethacin, and PLGA blended with indomethacin. While indomethacin alone exhibits a pronounced endothermic melting peak near 160 °C, this sharp melting peak is absent in the PLGA–indomethacin composite,[20] indicating a loss of crystallinity upon incorporation into the polymer.

Together, the FTIR and DSC results supported the successful incorporation of teicoplanin and indomethacin into the PLGA nanofibers.

3.3. *In vitro* release profiles of biodegradable nanofibers

The release behaviors of indomethacin and teicoplanin from the electrospun nanofibers were evaluated. Figure 10A and 10B illustrate the daily and cumulative release patterns, respectively. Both drugs exhibited a pronounced initial burst release on day 1, followed by a gradual, sustained decline in release rate. The initial burst is important for interpretation because rapid exposure to surface-associated drugs may affect early local cell responses and should be further evaluated in cytotoxicity and biological activity assays. The nanofibers maintained teicoplanin release above the minimum inhibitory concentration (2.0 μg/mL)[21] for over 30 days, and sustained indomethacin release for more than 13 days. Additionally, BMP-2 was released from the nanofibers for over 30 days, as shown in Figure 10C. The present study measured BMP-2 concentration but did not directly confirm retained BMP-2 bioactivity after release.

3.4. *In vivo* release

Figure 11 displays the *in vivo* release profiles of indomethacin and teicoplanin at multiple time points after implantation in healthy rabbits. In contrast to the *in vitro* profiles, a distinct initial burst was not observed in the measured tissue samples. The nanofibers maintained higher local than systemic concentrations of both pharmaceuticals for 28 days, supporting localized delivery from the implanted scaffold. On day 28 post-implantation, the PCL mesh remained visible, while the nanofibers had largely degraded (Figure 2C). These findings demonstrate local release behavior and partial degradation of the nanofibrous component but do not demonstrate inhibition of ectopic bone formation.

3.5. Histological evaluation

Figure 12 presents representative histological sections obtained at 1, 7, 14, and 28 days after implantation of the hybrid biodegradable scaffold. Histological examination demonstrated an early inflammatory response characterized by substantial infiltration of mononuclear inflammatory cells in the peri-implant tissue as early as postoperative day 1. By day 7, inflammatory cells, including polymorphonuclear leukocytes, lymphocytes, plasma cells, and eosinophils, were observed around the implanted scaffold. Subsequently, the inflammatory response gradually subsided, with progressive reductions in inflammatory cell density on days 14 and 28. Because histology was descriptive and did not include quantitative scoring, immunohistochemistry, or mineralization assessment, these results should be interpreted as preliminary biocompatibility observations rather than evidence of anti-inflammatory or anti-HO efficacy.

4. Discussion

In this study, we fabricated a hybrid biodegradable scaffold combining a solvent-cast 3D-printed PCL mesh with multilayer PLGA electrospun/coaxially electrospun nanofibers. The interpretation of this work is deliberately focused on material fabrication, mechanical characterization of both individual components and the assembled hybrid construct, and localized release behavior. Although the scaffold was designed for potential use in HO-prone peri-osseous environments, the present data do not directly demonstrate HO prevention because the *in vivo* implantation was performed in healthy rabbits and ectopic bone formation was not induced or quantified.

The main technical concept is the integration of two structural scales and multiple delivery compartments. The PCL mesh provides a flexible macro-scale framework that may act as a physical separator around bone, while PLGA nanofibers provide a high-surface-area carrier for localized drug release. The electrospun layers allowed delivery of indomethacin and teicoplanin, and the coaxial layer provided a separate compartment for BMP-2.

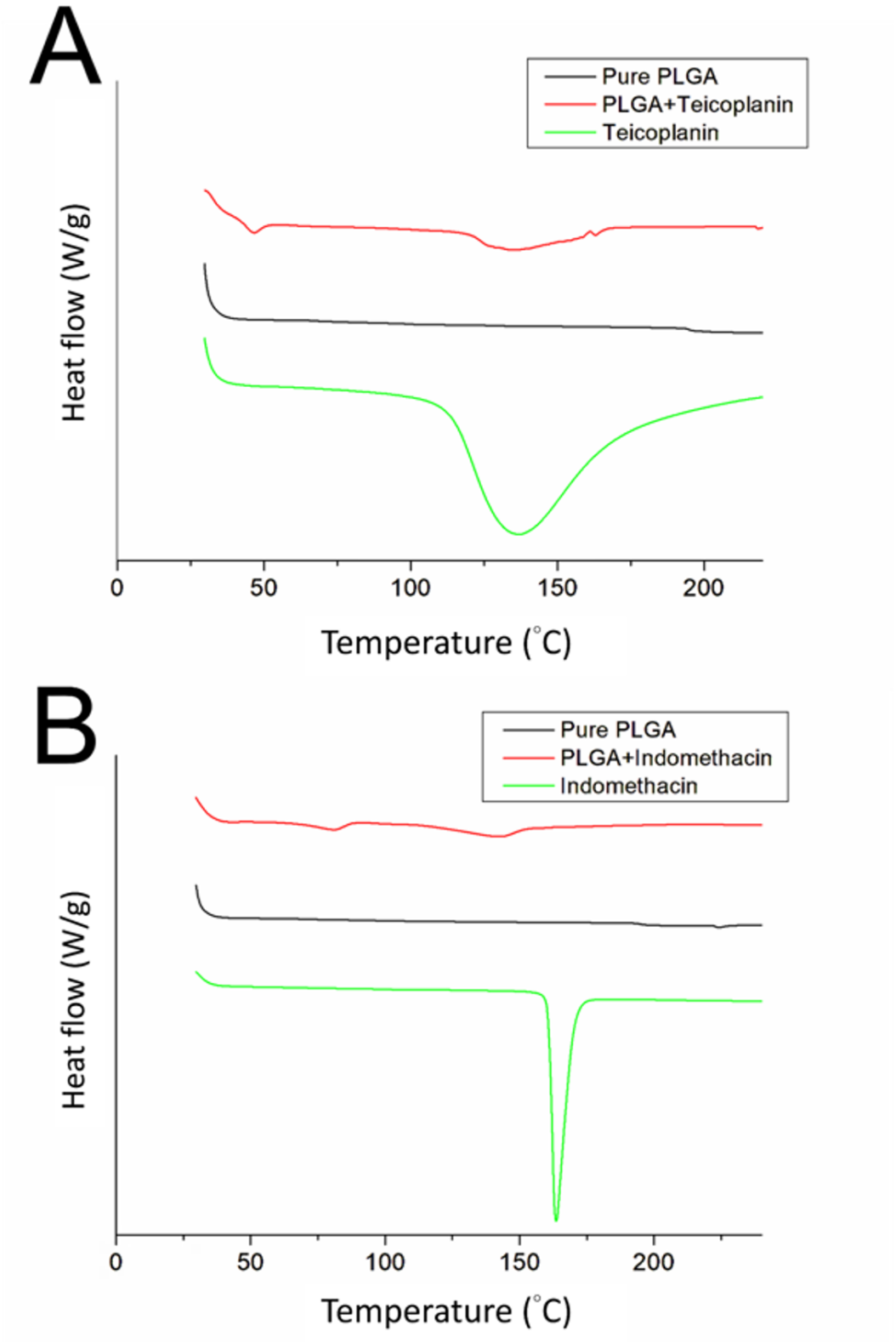

Figure 9. Differential scanning calorimetry thermograms of (A) poly(lactic-co-glycolic acid) (PLGA)/teicoplanin and (B) PLGA/indomethacin nanofibers

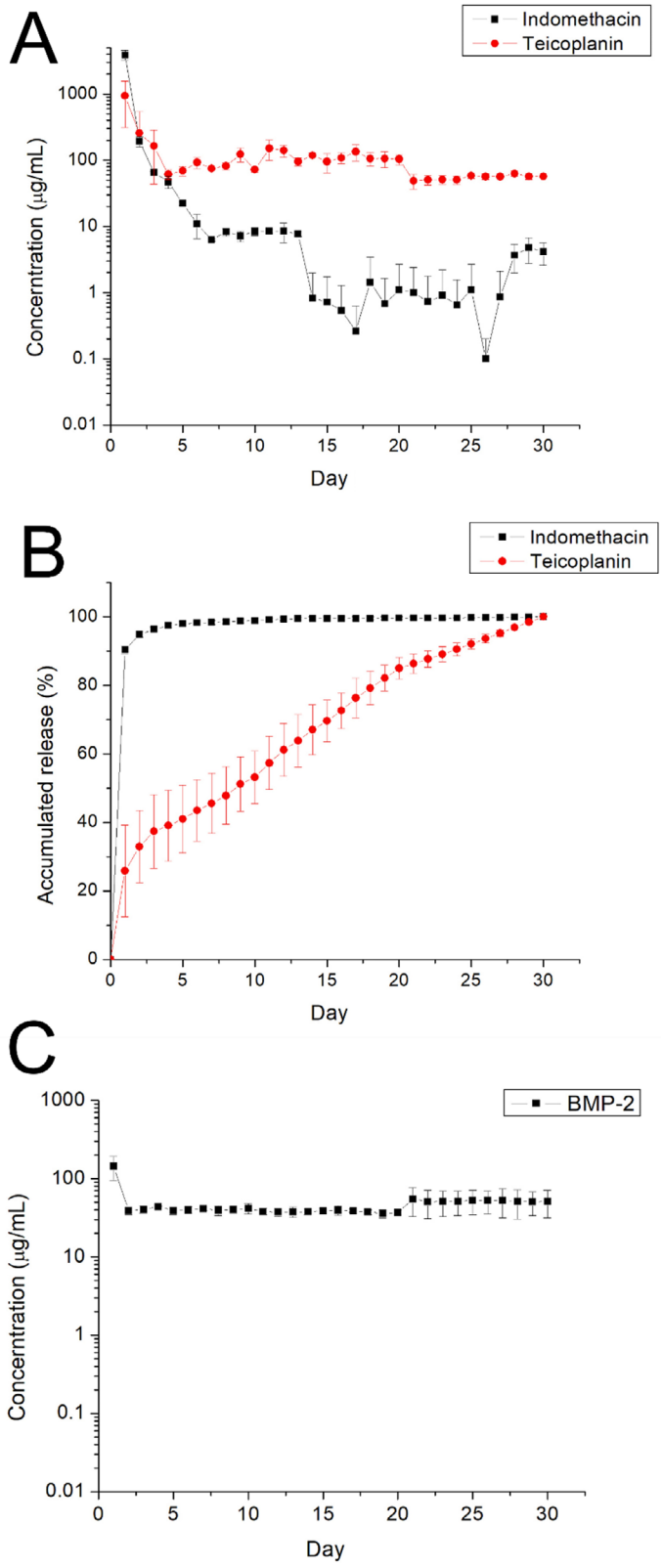

Figure 10. *In vitro* (A) daily and (B) cumulative elution profiles of teicoplanin and indomethacin, and (C) daily release of bone morphogenetic protein 2 (BMP-2) from the nanofibers

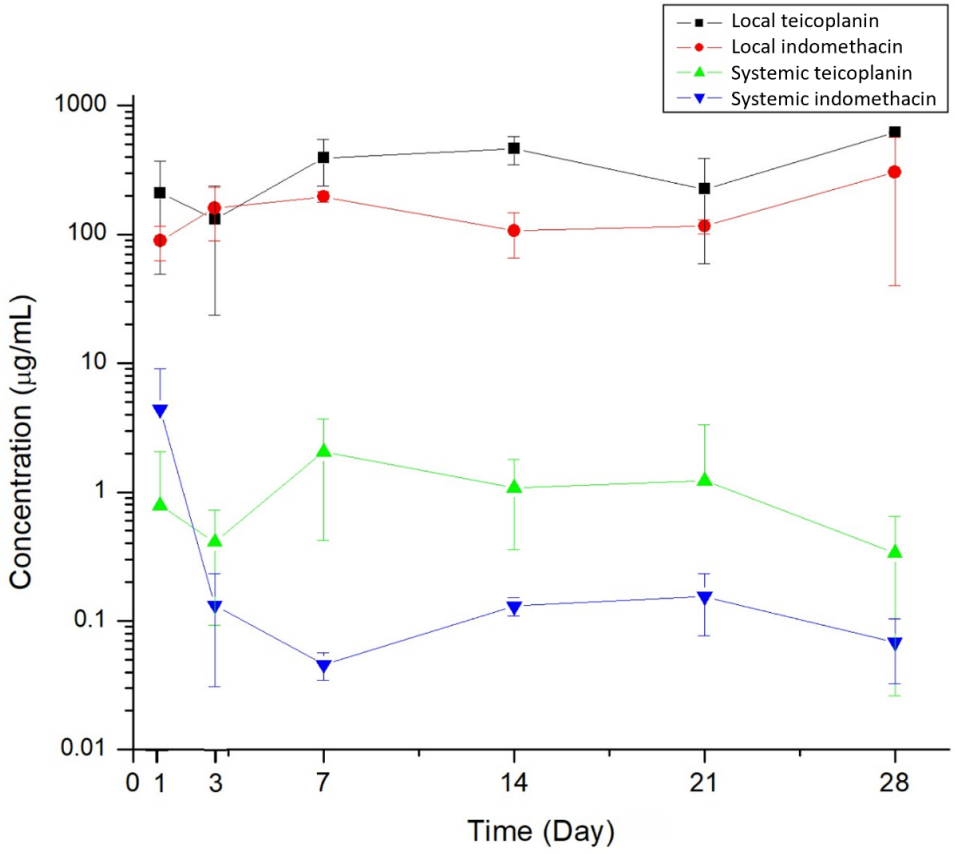

Figure 11. *In vivo* release profiles of teicoplanin and indomethacin after implantation in healthy rabbits. Local tissue concentrations were higher than systemic concentrations over 28 days. Data are presented as mean ± standard deviation.

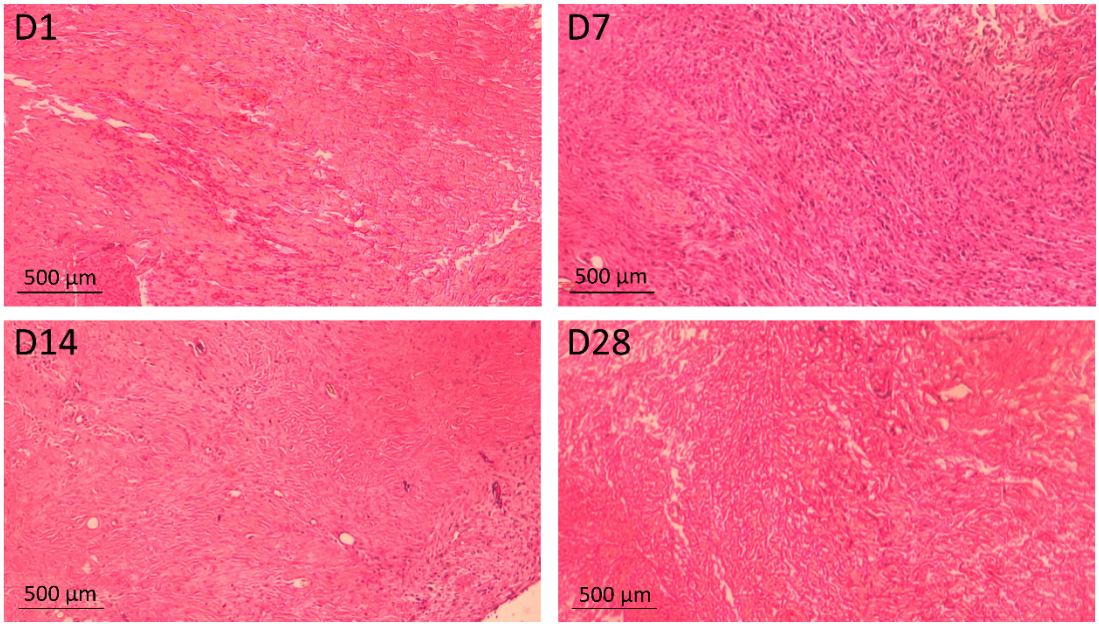

Figure 12. Representative hematoxylin and eosin-stained histological sections of peri-implant tissues at 1, 7, 14, and 28 days following implantation of the hybrid biodegradable drug-eluting scaffold. The sections show early peri-implant inflammatory-cell infiltration with gradual reduction over time. No quantitative histological scoring or ectopic mineralization assessment was performed. Scale bar = 500 μm; magnification: 40×.

This combined architecture differs from single-material membranes or drug carriers by attempting to combine barrier function, local anti-inflammatory/antibiotic release, and an exploratory bone-healing signal in one degradable construct. Nevertheless, this conceptual advantage requires direct comparison with appropriate controls in future studies, including PCL mesh alone, unloaded PLGA fibers, single-agent scaffolds, and free-drug treatment groups.

The selection of PCL and PLGA was based on their established use as biodegradable polymers in biomedical and drug-delivery applications. Biodegradable polymeric materials have been widely investigated for implantable devices, tissue engineering, and controlled drug delivery because they can provide temporary structural or delivery functions and subsequently degrade without requiring permanent retention in the body.[22,23] PCL was selected as the macro-scale mesh material because of its biocompatibility, processability, flexibility, and relatively slow degradation profile, which are favorable for maintaining a conformable peri-osseous barrier during the early postoperative period.[24,25] In contrast, PLGA was selected for the nanofibrous drug-delivery layers because its degradation behavior and release profile can be adjusted and because it has been widely used as a carrier for sustained therapeutic-agent delivery.[26,27] In the present scaffold design, PCL and PLGA therefore serve distinct but complementary functions: PCL provides the structural backbone and barrier-like support, whereas PLGA nanofibers provide localized drug delivery.

The fabrication strategy also reflects these functional requirements. Additive manufacturing enables the production of customized 3D structures with controlled geometry, porosity, and architecture, which is useful for fabricating macro-scale biomedical scaffolds.[28-30] Electrospinning, by contrast, produces ultrafine polymeric fibers with high surface area and porous morphology, making it suitable for drug incorporation and controlled release.[31] Coaxial electrospinning further allows the generation of core-shell nanofibers, which can protect sensitive bioactive molecules and provide an additional level of compartmentalized release control.[32] Therefore, the novelty of the present work should not be interpreted as the individual use of PCL, PLGA, 3D printing, electrospinning, or coaxial electrospinning, but rather as the integration of these established technologies into a single hybrid peri-osseous scaffold platform.

The release data support sustained local delivery but also highlight important safety and interpretation issues. *In vitro* testing showed a day-1 burst of indomethacin and teicoplanin, followed by sustained release. This pattern is common for electrospun fibers because surface-associated drug dissolves rapidly after exposure to aqueous media, whereas subsequent release is governed by diffusion and polymer degradation.[33,34] The *in vivo* measurements showed higher local than systemic drug concentrations over 28 days, suggesting that the scaffold can limit systemic exposure. However, the potential cytotoxicity of the burst release, the antibacterial activity of released teicoplanin, and the anti-inflammatory activity of released indomethacin were not tested in the present study and should be addressed before efficacy claims are made.

The BMP-2 component requires particularly cautious interpretation. In the present scaffold design, BMP-2 should be regarded as an exploratory component rather than a validated therapeutic element for HO-related treatment. BMP-2 is a potent osteoinductive factor that can promote osteogenic differentiation and bone formation; however, dysregulated BMP signaling is also closely implicated in the pathogenesis of HO. Therefore, although localized BMP-2 delivery may be beneficial when spatially confined to a bone-defect interface requiring regeneration, uncontrolled diffusion into surrounding soft tissues could theoretically increase the risk of ectopic bone formation. In the present study, BMP-2 release was quantified *in vitro*, but the retained bioactivity of released BMP-2, its spatial restriction within the peri-osseous region, its dose-dependent effects, and its interaction with concurrently released indomethacin were not evaluated. Accordingly, no therapeutic benefit of BMP-2 in HO-prone environments can be claimed based on the current data. Future studies should verify spatially restricted BMP-2 release, retained bioactivity after coaxial electrospinning, and the net biological response under combined BMP-2 and indomethacin exposure. These studies should include cell viability assays, ALP activity, mineralization assays such as Alizarin Red staining, and osteogenic-marker analysis to determine whether released BMP-2 remains bioactive and whether indomethacin modifies the osteogenic response.

The wettability results also support the role of nanofiber composition in modulating scaffold surface properties. Surface hydrophilicity can influence protein adsorption, cell attachment, and early tissue interaction with biomaterials.[35,36] In the present study, pristine PLGA nanofibers were relatively hydrophobic, whereas incorporation of teicoplanin markedly decreased the water contact angle, likely because of the higher water solubility of teicoplanin. Indomethacin and BMP-2 loading produced less pronounced changes in wettability. Although these findings suggest that drug incorporation can alter the surface characteristics of PLGA nanofibers, the present study did not directly assess cell adhesion, proliferation, or cytocompatibility; therefore, the biological implications of

these wettability changes require further investigation.

The additional mechanical testing of the assembled hybrid scaffold provides important information beyond component-level characterization. In the scaffold design, the PCL mesh is intended to serve as the macro-scale structural backbone and conformable barrier, whereas the PLGA nanofibrous membranes primarily function as drug-delivery compartments. Therefore, the overall behavior of the final construct cannot be fully inferred from PCL mesh or PLGA nanofiber testing alone. After PBS immersion for 3 days, the PCL mesh/PLGA nanofiber hybrid scaffold demonstrated a stress-strain response broadly comparable to that of the PCL mesh alone, with only a modest reduction in ultimate tensile strength (24.8 ± 2.0 MPa versus 26.2 ± 2.6 MPa) and preserved maximum strain (334 ± 6% versus approximately 337%). This result suggests that the mechanical behavior of the assembled scaffold is mainly governed by the 3D-printed PCL mesh and that integration of the PLGA nanofibrous layer does not markedly impair flexibility or tensile integrity under hydrated conditions. Because the scaffold is designed as a conformable peri-osseous drug-delivery and barrier platform rather than a load-bearing fixation device, preservation of handling integrity, flexibility, and extensibility is more clinically relevant than high load-bearing strength. Nevertheless, longer-term wet-state mechanical testing during polymer degradation remains necessary to evaluate construct durability throughout the intended release period.

The histological findings showed an early inflammatory response that gradually decreased by day 28. This pattern is compatible with a tissue response to an implanted biodegradable material, but the assessment was descriptive. The absence of quantitative inflammatory scoring, immunohistochemistry, macrophage polarization markers, osteogenic markers, fibrosis assessment, and ectopic mineralization analysis prevents mechanistic conclusions. Similarly, because no micro-computed tomography, radiography, histomorphometry, or functional outcome measures were performed in an HO model, the study cannot determine whether the scaffold reduces ectopic bone volume or improves function.

This study has several limitations. First, the animal experiment was conducted in healthy rabbits rather than in a validated HO model. Second, the *in vivo* sample size was small, and the analysis focused on local and systemic drug concentrations rather than disease efficacy. Third, no clinically relevant control groups were included, such as PCL mesh alone, unloaded PLGA nanofibers, single-agent scaffolds, or free-drug treatment groups. Fourth, although the theoretical loading amounts of indomethacin, teicoplanin, and BMP-2 were determined based on the quantities of drugs, biomolecules, and polymer used during scaffold fabrication, the actual total loaded amount, drug-loading efficiency, and encapsulation efficiency were not directly quantified. Therefore, the current release profiles should be interpreted as preliminary release-characterization data rather than optimized dose-delivery profiles. Direct measurement of total loaded amount, loading efficiency, encapsulation efficiency, and cumulative percentage release for each agent will be required in future studies for dose optimization, batch-to-batch quality control, and translational evaluation. Fifth, although short-term PBS-conditioned tensile testing of the assembled hybrid scaffold was added, long-term wet-state mechanical behavior during polymer degradation, residual solvent quantification, toxicity assessment, and dose optimization were not fully assessed. Sixth, the biological activities of released BMP-2, teicoplanin, and indomethacin were not tested using osteogenic, antibacterial, anti-inflammatory, or cytotoxicity assays. These limitations substantially restrict translational interpretation.

Accordingly, the present scaffold should be regarded as a prototype localized peri-osseous drug-delivery and barrier platform rather than a proven anti-HO therapy. Future work should use validated HO models, such as trauma- or burn-associated models, and should include micro-computed tomography quantification of ectopic bone, radiographic assessment, histomorphometry, biological-marker analysis, and functional outcomes. Appropriate material and pharmacologic controls will be essential to determine the contribution of each component and to clarify whether the addition of BMP-2 is beneficial or potentially harmful in an HO-prone environment. In addition, comprehensive drug-loading and release-characterization studies will be necessary to establish reproducible dosing, define therapeutic windows, and support future translational development of this platform.

Overall, the data support the feasibility of fabricating a degradable hybrid scaffold and achieving sustained local release with relatively low systemic exposure. The findings provide a basis for further optimization but should not be interpreted as direct evidence of HO mitigation.

5. Conclusion

In this study, we developed a biodegradable hybrid scaffold combining a 3D-printed PCL mesh with drug-loaded PLGA nanofibrous membranes as a localized peri-osseous drug-delivery platform for HO-related applications. The scaffold incorporates design features relevant to HO management, including a conformable physical barrier, sustained local release of indomethacin for inflammatory modulation, teicoplanin for local infection control,

and BMP-2 for bone-regenerative support. The scaffold demonstrated feasible fabrication, favorable flexibility of the PCL mesh, preserved wet-state tensile behavior of the assembled PCL mesh/PLGA nanofiber hybrid construct after PBS immersion, sustained *in vitro* release of indomethacin, teicoplanin, and BMP-2, and sustained local release of indomethacin and teicoplanin over 28 days in healthy rabbits with relatively low systemic exposure. The assembled hybrid scaffold retained an ultimate tensile strength of 24.8 ± 2.0 MPa and a maximum strain of 334 ± 6%, supporting its handling integrity as a conformable peri-osseous platform. These findings support the scaffold as a promising preliminary platform for localized modulation of the peri-osseous environment in HO-risk settings. Nevertheless, because no validated HO model, ectopic bone quantification, or mechanistic biological assays were performed, its direct ability to prevent or reduce HO remains unproven and requires further disease-model efficacy and safety studies.

Acknowledgments

None.

Funding

This work was supported in part by the National Science and Technology Council, Taiwan (Contract No. 114-2221-E-182-003-MY3) and the Chang Gung Memorial Hospital (Contract No. CMRPD2M0012).

Conflict of interest

The authors declare no conflict of interest.

Author contribution

Conceptualization: Chih-Yang Lai, Po-Ju Lai
Formal analysis: Zi-He Kuo, Ulfia Nur Amallia
Investigation: Szu-Yao Wang, Shih-Jung Liu
Methodology: Po-Ju Lai, I-Lan Fan
Writing–original draft: Chih-Yang Lai
Writing–review & editing: Shih-Jung Liu

Ethics approval and consent to participate

All animal experiments were approved by the Institutional Animal Care and Use Committee of Chang Gung University (IACUC No.: CGU113-178). No human participants or human-derived materials were involved.

Consent for publication

Not applicable.

Availability of data

The datasets generated and analyzed during the current study are available from the corresponding author upon reasonable request.

References

1. Ranganathan K, Loder S, Agarwal S, *et al*. Heterotopic ossification: basic-science principles and clinical correlates. *J Bone Joint Surg Am*. 2015;97(13):1101-1111.

   doi: 10.2106/JBJS.N.01056

2. Meyers C, Lisiecki J, Miller S, *et al*. Heterotopic ossification: a comprehensive review. *JBMR Plus*. 2019;3(4):e10172.

   doi: 10.1002/jbm4.10172

3. Ramirez DM, Ramirez MR, Reginato AM, Medici D. Molecular and cellular mechanisms of heterotopic ossification. *Histol Histopathol*. 2014;29(10):1281-1285.

   doi: 10.14670/HH-29.1281

4. Bei M, Cao Q, Zhao C, Wu X. Heterotopic ossification: current developments and emerging potential therapies. *Chin Med J (Engl)*. 2025;138(4):389-404.

   doi: 10.1097/CM9.0000000000003244

5. Felix-Ilemhenbhio F, Pickering GAE, Kiss-Toth E, Wilkinson JM. Pathophysiology and emerging molecular therapeutic targets in heterotopic ossification. *Int J Mol Sci*. 2022;23(13):6983.

   doi: 10.3390/ijms23136983

6. Zhou L, Gee SM, Hansen JA, Posner MA. Heterotopic ossification after arthroscopic procedures: a scoping review of the literature. *Orthop J Sports Med*. 2022;10(1):23259671211060040.

   doi: 10.1177/23259671211060040

7. Kontokostopoulos AP, Gkiatas I, Vasileiadis GI, *et al*. Heterotopic ossification around the elbow revisited. *Life (Basel)*. 2023;13(12):2358.

   doi: 10.3390/life13122358

8. Pakos EE, Ioannidis JPA. Radiotherapy vs nonsteroidal anti-inflammatory drugs for the prevention of heterotopic ossification after major hip procedures: a meta-analysis of randomized trials. *Int J Radiat Oncol Biol Phys*. 2004;60(3):888-895.

   doi: 10.1016/j.ijrobp.2003.11.015

9. Geller JS, Allegra PR, Seldon CS, *et al*. Prophylactic radiotherapy for prevention of heterotopic ossification after periacetabular fractures: a review of efficacy and associated conditions. *J Surg Orthop Adv*. 2022;31(2):113-118. PMID:35820098

10. Georhakopoulos I, Kouloulias V, Kougiountzopoulou A, *et al*. Radiation therapy for the prevention of heterotopic ossification: efficacy and toxicity of single-fraction radiotherapy. *Orthop Rev (Pavia)*. 2020;12(2):8577.

doi: 10.4081/or.2020.8577

11. Zhao P, Gu H, Mi H, Rao C, Fu J, Turng LS. Fabrication of scaffolds in tissue engineering: a review. *Front Mech Eng*. 2018;13(1):107-119.

    doi: 10.1007/s11465-018-0496-8

12. Almouemen N, Kelly HM, O'Leary C. Tissue engineering: understanding the role of biomaterials and biophysical forces on cell functionality through computational and structural biotechnology analytical methods. *Comput Struct Biotechnol J*. 2019;17:591-598.

    doi: 10.1016/j.csbj.2019.04.008

13. Ganesan O, Kiwanuka H, Hamaguchi R, Orgill DP. A review of regenerative medicine and tissue engineering with a focus on wound healing and anti-aging. *Front Surg*. 2025;12:1504563.

    doi: 10.3389/fsurg.2025.1504563

14. Chen JM, Lee D, Yang JW, Lin SH, Lin YT, Liu SJ. Solution extrusion additive manufacturing of biodegradable polycaprolactone. *Appl Sci*. 2020;10(9):3189.

    doi: 10.3390/app10093189

15. Sayet G, Sinegre M, Reguiga MB. Development of a Fourier transform infrared spectroscopy coupled to UV-Visible analysis technique for aminosides and glycopeptides quantitation in antibiotic locks. *Ann Pharm Fr*. 2014;72(1):41-50.

    doi: 10.1016/j.pharma.2013.10.002

16. Amiri N, Ajami S, Shahroodi A, *et al*. Teicoplanin-loaded chitosan-PEO nanofibers for local antibiotic delivery and wound healing. *Int J Biol Macromol*. 2020;162:645-656.

    doi: 10.1016/j.ijbiomac.2020.06.195

17. Liu M, Liu J, Wang Q, *et al*. Quantitative analysis of amorphous form in indomethacin binary polymorphic mixtures using infrared spectroscopy analytical techniques combined with chemometrics methods. *Arab J Chem*. 2023;16(8):104885.

    doi: 10.1016/j.arabjc.2023.104885

18. Otsuka Y, Kuwashima W, Tanaka Y, Yamaki Y, Shimada Y, Goto S. Effects of heat treatment on indomethacin-cimetidine mixture: investigation of drug-drug interaction using singular value decomposition in FTIR spectroscopy. *J Pharm Sci*. 2021;110(3):1142-1147.

    doi: 10.1016/j.xphs.2020.09.049

19. Flieger J, Orzel A, Kowalska-Kepczynska A, *et al*. Teicoplanin-modified HPLC column as a source of experimental parameters for prediction of the anticonvulsant activity of 1,2,4-triazole-3-thiones by the regression models. *Materials (Basel)*. 2020;13(11):2650.

    doi: 10.3390/ma13112650

20. Ornik J, Heidrich L, Schesny R, Castro-Camus E, Keck CM, Koch M. Non-destructive crystallinity assessment of indomethacin in tablets made from smartFilms using terahertz time-domain spectroscopy. *Sci Rep*. 2022;12(1):6099.

    doi: 10.1038/s41598-022-10041-1

21. Liu CY, Lee WS, Fung CP, *et al*. Comparative study of teicoplanin vs vancomycin for the treatment of methicillin-resistant Staphylococcus aureus bacteraemia. *Clin Drug Investig*. 1996;12(2):80-87.

    doi: 10.2165/00044011-199612020-00003

22. Song R, Murphy M, Li C, Ting K, Soo C, Zheng Z. Current development of biodegradable polymeric materials for biomedical applications. *Drug Des Devel Ther*. 2018;12:3117-3145.

    doi: 10.2147/DDDT.S165440

23. Kalirajan C, Dukle A, Nathanael AJ, Oh TH, Manivasagam G. A critical review on polymeric biomaterials for biomedical applications. *Polymers (Basel)*. 2021;13(17):3015.

    doi: 10.3390/polym13173015

24. Woodruff MA, Hutmacher DW. The return of a forgotten polymer-polycaprolactone in the 21st century. *Prog Polym Sci*. 2010;35(10):1217-1256.

    doi: 10.1016/j.progpolymsci.2010.04.002

25. Backes EH, Harb SV, Beatrice CAG, *et al*. Polycaprolactone usage in additive manufacturing strategies for tissue engineering applications: a review. *J Biomed Mater Res B Appl Biomater*. 2022;110(6):1479-1503.

    doi: 10.1002/jbm.b.34997

26. Yang J, Zeng H, Luo Y, *et al*. Recent applications of PLGA in drug delivery systems. *Polymers (Basel)*. 2024;16(18):2606.

    doi: 10.3390/polym16182606

27. Marquina S, Ozgul M, Robertson-Brown K, Kenney MC. A review on PLGA particles as a sustained drug-delivery system and its effect on the retina. *Exp Eye Res*. 2023;235:109626.

    doi: 10.1016/j.exer.2023.109626

28. Ngo TD, Kashani A, Imbalzano G, Nguyen KTQ, Hui D. Additive manufacturing (3D printing): a review of materials, methods, applications and challenges. *Compos B Eng*. 2018;143:172-196.

    doi: 10.1016/j.compositesb.2018.02.012

29. Rasiya G, Shukla A, Saran K. Additive manufacturing-a review. *Mater Today Proc*. 2021;47:6896-6901.

    doi: 10.1016/j.matpr.2021.05.181

30. Bozkurt Y, Karayel E. 3D printing technology; methods, biomedical applications, future opportunities and trends. *J Mater Res Technol*. 2021;14:1430-1450.

    doi: 10.1016/j.jmrt.2021.07.050

31. Xue J, Wu T, Dai Y, Xia Y. Electrospinning and electrospun nanofibers: methods, materials, and applications. *Chem Rev*. 2019;119(8):5298-5415.

doi: 10.1021/acs.chemrev.8b00593

32. Zhao J, Chen L, Ma A, *et al*. Recent advances in coaxial electrospun nanofibers for wound healing. *Mater Today Bio*. 2024;29:101309.

doi: 10.1016/j.mtbio.2024.101309

33. Ali SA, Doherty PJ, Williams DF. Mechanisms of polymer degradation in implantable devices. 2. Poly(DL-lactic acid). *J Biomed Mater Res*. 1993;27(11):1409-1418.

doi: 10.1002/jbm.820271108

34. Kamaly N, Yameen B, Wu J, Farokhzad OC. Degradable controlled-release polymers and polymeric nanoparticles: mechanisms of controlling drug release. *Chem Rev*. 2016;116(4):2602-2663.

doi: 10.1021/acs.chemrev.5b00346

35. Benhabbour SR, Sheardown H, Adronov A. Cell adhesion and proliferation on hydrophilic dendritically modified surfaces. *Biomaterials*. 2008;29(31):4177-4186.

doi: 10.1016/j.biomaterials.2008.07.016

36. Torres E, Valles-Lluch A, Fombuena V, Napiwocki B, Turng LS. Influence of the hydrophobic-hydrophilic nature of biomedical polymers and nanocomposites on in vitro biological development. *Macromol Mater Eng*. 2017;302(12):1700259.

doi: 10.1002/mame.201700259